ChemPubSoc Europe

DOI: 10.1002/chem.201406126

CHEMISTRY A European Journal Full Paper

Composite Materials

Chemical versus Electrochemical Synthesis of Carbon Nano-onion/Polypyrrole Composites for Supercapacitor Electrodes

Olena Mykhailiv,[a] Monika Imierska,[a] Martyna Petelczyc,[a] Luis Echegoyen,*[b] and Marta E. Plonska-Brzezinska*[a]

Abstract: The development of high-surface-area carbon electrodes with a defined pore size distribution and the incorporation of pseudo-active materials to optimize the overall capacitance and conductivity without destroying the stability are at present important research areas. Composite electrodes of carbon nano-onions (CNOs) and polypyrrole (Ppy) were fabricated to improve the specific capacitance of a supercapacitor. The carbon nanostructures were uniformly coated with Ppy by chemical polymerization or by electrochemical potentiostatic deposition to form homogenous composites or bilayers. The materials were characterized by transmission- and scanning electron microscopy, differential thermogravimetric analyses, FTIR spectroscopy, piezoelectric microgravimetry, and cyclic voltammetry. The composites show higher mechanical and electrochemical stabilities, with high specific capacitances of up to about 800 $F g^{-1}$ for the CNOs/SDS/Ppy composites (chemical synthesis) and about 1300 $F g^{-1}$ for the CNOs/Ppy bilayer (electrochemical deposition).

Introduction

Carbon nanostructures have attracted considerable attention because of their unique physical and chemical properties. They show high chemical stability and large specific surface area. The integration of carbon materials with polymers,[1] biomolecules,[2] inorganic materials,[3] or polyelectrolytes[4] has led to the development of new materials and sensors. The combination of carbon materials with conducting polymers results in novel materials with potential practical applications. The development of composites for use as supercapacitor electrodes (CEs) can provide enhanced potential electronic and ionic conductivity, and can considerably improve charge storage and delivery. The fabrication of composites by using carbon materials as a support increases the effective utilization of the active materials and improve the electrical conductivity. This combination offers also attractive possibilities to reinforce polymers to improve their mechanical properties.

Generally, on the basis of the energy storage mechanism, supercapacitors can be classified into two types. The charge on the electrode surface/electrolyte interface can be stored by electrostatic interactions (electrical double layer capacitors, EDLCs) or by faradaic processes (pseudocapacitors, PCs). In EDLCs the capacitance arises from pure electrostatic accumulation of charge at the electrode/electrolyte interface.[5] The capacitance is strongly dependent on the surface area of the electrode material that is accessible to the electrolyte ions. The electrode materials in PCs are electrochemically active and fast faradaic reactions are involved, requiring charge transfer across the double layer.[6]

The carbon-based electrode materials possess unique chemical and physical properties, namely: 1) reasonably high conductivity; 2) relatively high surface-area; 3) high thermal stability; 4) excellent corrosion resistance; 5) controlled pore size distribution; and 6) compatibility with composite materials.[7] Although they show many advantages, the non-modified carbon surfaces show limited accessibility to the electrolyte in EDLCs and affects the performance of supercapacitors. An effective approach is to modify the carbon surface with redox materials, such as transition-metal oxides,[8] and conducting polymers,[9,13] to form composites. Composite materials based on the integration of carbon structures with other substances can lead to materials possessing properties of the individual components: the large pseudocapacitance from the redox-capacitive materials and the robustness of the carbon nanostructures provide promising applications for electrochemical or photovoltaics purposes.[10] The challenge is the fabrication of composite materials containing conducting polymers and carbon materials with the proper ratio of components and a homogeneous structure. Different porous carbon nanostructures have been used as supports for the deposition of electroactive conducting polymers, that is, polyaniline,[11] polypyrrole (Ppy),[12] and

[a] O. Mykhailiv, M. Imierska, M. Petelczyc, Dr. M. E. Plonska-Brzezinska
Institute of Chemistry, University of Bialystok
Hurtowa 1, 15-399 Bialystok (Poland)
Fax: (+48-85) 747-0113
E-mail: mplonska@uwb.edu.pl

[b] Prof. Dr. L. Echegoyen
Department of Chemistry, University of Texas at El Paso
500W University Ave., El Paso, TX 79968 (USA)
Fax: (+1-915) 747-8807
E-mail: echegoyen@utep.edu

Supporting information for this article is available on the WWW under http://dx.doi.org/10.1002/chem.201406126.

© 2015 Wiley-VCH Verlag GmbH & Co. KGaA, Weinheim

their derivatives to prepare carbon/conductive composite electrodes.

Polypyrrole is one of the best known materials as it exhibits relatively high conductivity, good stability in water and air, and relatively low cost.[13–15] The redox transitions of PPy can occur within the available potential window for water at neutral pH,[16] which is less corrosive than the strongly acidic electrolytes employed for PANI.[17] On the other hand, PPy exhibits poor cycling stability during the charge–discharge processes.

Ppy can be easily prepared using either chemical[18] or electrochemical[19] methods. There are different advantages for each method. Chemical synthesis requires oxidants. The electrochemical methods, including potentiostatic, galvanostatic, and potential-cycling methods, are preferred for electrode preparation because the conducting polymers can be directly coated on the substrates and they exhibit much better electrical conductivity than materials prepared chemically. Since PPy is polymerized by electrochemical techniques onto the electronically conductive substrates, the capacitive properties of the synthesized polymers are strongly dependent on the counterions present during the polymerization.[20] Accordingly, the effects of preparation variables on the capacitive performance and textural properties of PPy are worth studying. On the other hand, chemical synthesis results in materials showing lower homogeneity. Since the chemical polymerization results in a more porous morphology of the polymers, the degree of solvent swelling and ion transport through the obtained films is easier.[21]

The supercapacitors have been developed to combine different electrode materials to improve device performances. Polypyrrole and carbon composites are promising electrode materials for this purpose. For example, well-defined core–shell carbon black/polypyrrole composites were prepared by in situ chemical oxidative polymerization. A maximum discharge capacity for this composite of 366 $F g^{-1}$ was achieved.[22] The composite materials containing 20 wt% of multiwalled carbon nanotubes and 80 wt% of chemically formed conducting polymers such as polypyrrole have been prepared. In the case of three-electrode cells, the highest capacitance values found were about 500 $F g^{-1}$. A remarkable specific capacitance of 427 $F g^{-1}$ was achieved for multi-walled carbon nanotube/polypyrrole membranes.[23] The electrochemical performance of graphene/polypyrrole composites has also been measured and a specific capacitance of 400 $F g^{-1}$ and 324 $F g^{-1}$ at a current density of 0.3 $A g^{-1}$ and 1.5 $A g^{-1}$ has been reported repeatedly.[24] Graphene nanolayers deposited by electrophoresis with Ppy attached on their surfaces, lead to specific capacitances up to 1510 $F g^{-1}$.[25] Chemical and electrochemical methods could be easily applied for the synthesis of PPy/carbon composites, and the correlation between the synthesis method and the physicochemical properties (mainly electrochemical) should be established.

Recently, we have focused on the synthesis of small carbon nano-onions (CNOs) structures (few shells), which can be compared to those of smaller single shelled structures such as C_{60} or larger ones, such as the carbon nanotubes. Our interest is the application of CNOs in supercapacitor electrodes. CNOs are spherical structures first observed by Iijima in amorphous carbon films prepared by a vacuum evaporation method.[26] Carbon nano-onion structures consist of a hollow spherical fullerene core surrounded by concentric fullerene layers with increasing diameter with a distance between the layers of 0.335 nm, which is very close to the interlayer distance in bulk graphite.[27] Different synthetic methods that start with various precursors lead to the preparation of CNOs, mainly differing in the number of layers and the nature of the core.[28,29] The following techniques have been reported for the synthesis of CNOs: electron-beam irradiation,[26,30] carbon-ion implantation,[31] thermal annealing of ultradispersed nanodiamond,[32] arc-discharge between two electrodes in water,[33] and chemical vapor deposition.[34] The method we use in our laboratory is based on thermal annealing of ultradispersed nanodiamond (ND) particles of about 5 nm in average diameter.[35] The resulting CNOs consist of a few graphene shells (6–8 layers). Recent studies of onion-like structures show very interesting physicochemical properties of these structures that are attractive for many applications.[36–38] CNOs have potential applications in energy conversion and storage,[39] catalysis,[40] electronics,[41,42] as cathodes in Li-ion electrochemical energy storage devices,[43,44] as optical limiting agents,[45–47] as hyperlubricants,[48,49] as electron field emitters,[50] and for biosensors.[2,51,52] Much attention has also been paid to the preparation of CNO composites with polymers,[51,53] solid polyelectrolytes,[4] metal oxides/hydroxides,[54] and metal nanoparticles.[55] The composites including CNOs show excellent properties such as long cycle life and highly reversible capacity.[56] Liu et al. investigated Ni/C nanocapsules with CNO shells as anode materials for lithium ion batteries.[58] This core–shell material exhibited excellent properties, such as a high charge–discharge rate and cycling stability.

Recently, we developed chemical and electrochemical procedures for the formation of composites containing CNOs and polypyrrole. Herein, we report the chemical and electrochemical synthesis and capacitance performance of new composite electrodes, namely CNOs/SDS/Ppy (Scheme 1a, (2)) and CNOs/Ppy (Scheme 1a, (1) and Scheme 1b). In this work we focus on a comparison of the electrochemical properties of the electrochemically and chemically synthesized composites. The effect of the different synthetic procedures on the morphology and electrochemical properties of Ppy, CNO/Ppy, and CNOs/SDS/Ppy was investigated. The specific capacitances of the resulting electrodes under various conditions are also reported.

Results and Discussion

Chemical preparation and characterization of CNO/PPy composites

The CNOs and polypyrrole composites were synthesized by the chemical polymerization of pyrrole (py), where pristine (Scheme 1a, (1)) and sodium dodecyl sulfate (SDS) functionalized CNOs (Scheme 1a, (2)) were used as the starting materials. In both procedures, 0.12 M $FeCl_3$ and 0.03 M pyrrole were used as the starting materials. The CNO particles were dispersed in

© 2015 Wiley-VCH Verlag GmbH & Co. KGaA, Weinheim

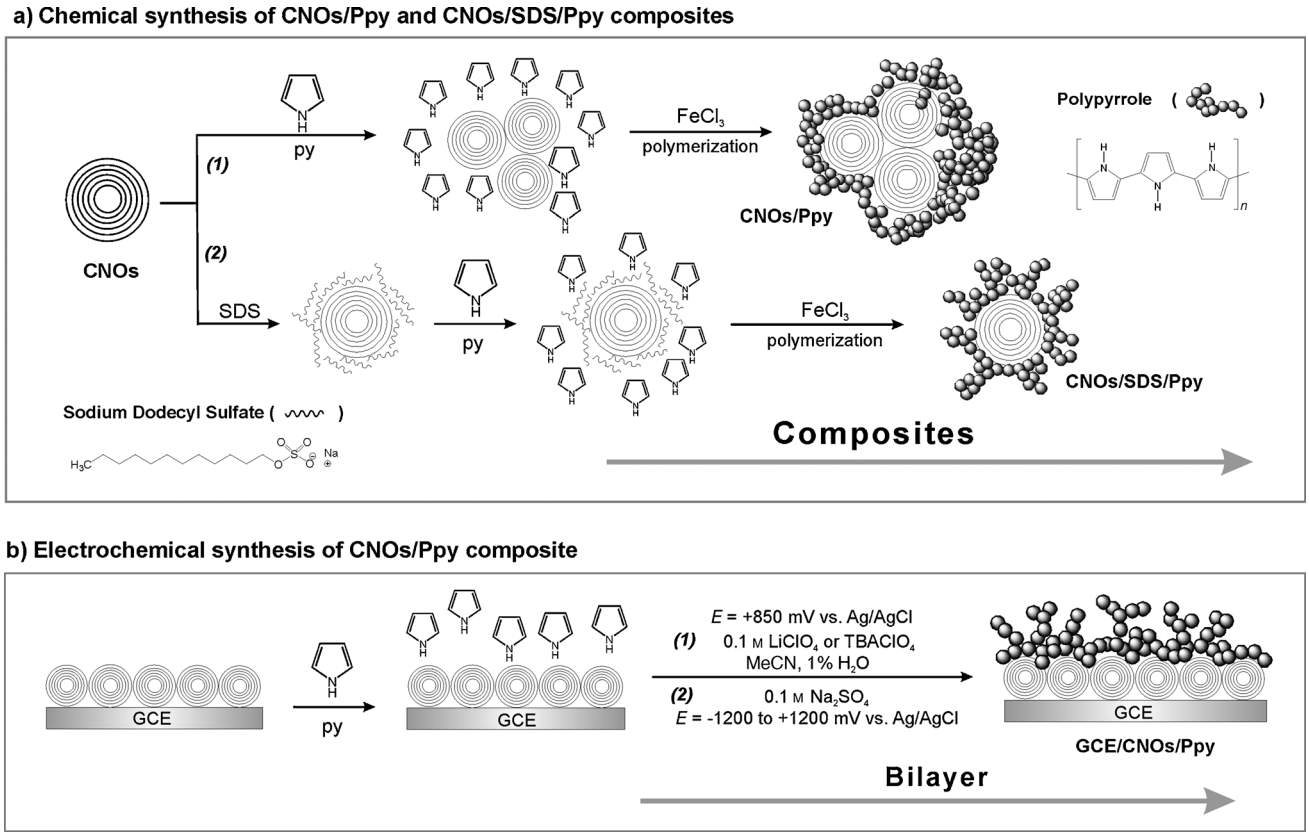

Scheme 1. a) The chemical synthesis of CNOs/Ppy and CNOs/SDS/PPy. b) The electrochemical polymerization of py at the GCE/CNOs electrode.

an aqueous solution (0.35 mg mL^{-1}) with SDS (3.75 10^{-7} g mL^{-1}). In this procedure, the negatively charged functional groups electrostatically interact with the pyrrole monomers, providing nucleation centers for the subsequent polymerization of pyrrole.

The TEM images shown in Figures 1a and 1b confirm the formation of the Ppy particles on the CNO surface. The morphologies of Ppy depend on the preparation conditions. Morphological characterization was performed to evaluate the degree of dispersion of the materials. SEM images of a Au foil covered with films of the CNOs/SDS/Ppy composites are shown in Figures 1e and 1f. Films were prepared by drop coating: 1.5 mg of CNOs or CNOs/SDS/Ppy was dispersed in 1 mL dichloromethane, and 20 μL of dispersion was transferred to a Au surface and evaporated. The morphology of the composites differs from the morphology of films formed only by the CNOs (Figure 1c). At the micrometer scale, CNOs form aggregates on the gold surface. Plain CNOs tend to agglomerate, which results from the van der Waals interactions between the nanoparticles (Scheme 1a, (1)). From Figure 1d, it can be seen that pristine Ppy synthesized without carbon nanostructures shows a typical granular morphology. The granule size of the pristine Ppy is about 0.3–0.5 μm. From the TEM images it was found that the CNO/Ppy composites consist of a large amount of pure polymer forming granular sheets and big aggregates of the carbon nanoparticles. The synthesis of the CNO/Ppy composites in the presence of SDS resulted in a good dispersion of CNOs and allowed a more uniform polymerization of pyrrole on the CNOs surface. Figure 1e and f reveal that the CNOs are uniformly coated with Ppy, indicating that the chemical polymerization of pyrrole was effectively achieved. The CNOs/SDS/PPy composite films show uniform morphology and porous structures with regular spherical, granular polymer particles deposited on the carbon materials (Figures 1e and 1f).

The thermal stabilities of the composites were determined by differential thermogravimetric analyses (TGA-DTG-DTA). The presence of both components, the carbon nanostructures as well as polymer phase were also confirmed by this method. The onset oxidation, inflection, and end temperatures are listed in Table 1, representing the initial weight loss, the maximum weight loss, and the final weight in the TGA-DTG-DTA graphs, respectively.

Figure 2 shows the TGA-DTG-DTA scans under an air atmosphere at 10 °C min^{-1} for CNOs, Ppy, and two composites: CNOs/Ppy and CNOs/SDS/Ppy. The temperature necessary for the removal of the porous carbon formed during the low-temperature annealing in an air atmosphere is lower than the combustion temperature of the pristine carbon nanostructures. As shown in Figure 2a and 2b, curve 1, CNOs exhibit a complete degradation at around 700 °C (see also Table 1) with an inflection temperature around 650 °C. The degradation process results from the combustion of CNOs in air. Analogous thermogravimetric analyses in an inert atmosphere (N_2) showed that the carbon nanoparticles were thermally stable up to

© 2015 Wiley-VCH Verlag GmbH & Co. KGaA, Weinheim

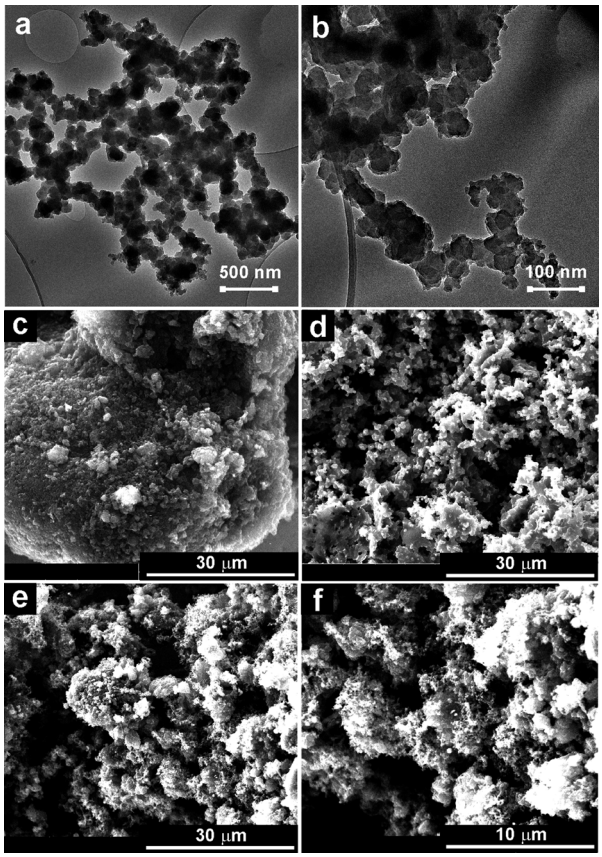

Figure 1. TEM images of a), b) CNOs/SDS/PPy and SEM images of c) CNOs, d) PPy, and e), f) CNOs/SDS/PPy.

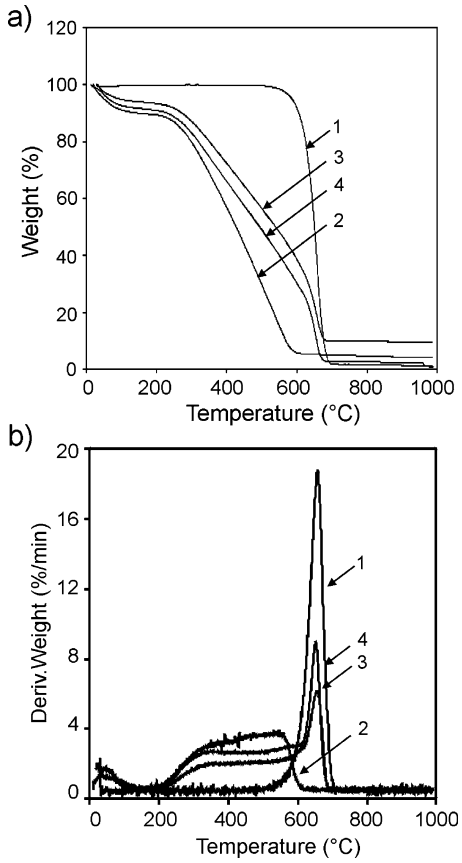

Figure 2. a) TGA and b) DTG curves of 1) CNOs, 2) Ppy, 3) CNOs/PPy, and 4) CNOs/SDS/PPy. Measurements in an air atmosphere at 10 °C min^{-1}.

Table 1. TGA-DTG-DTA results of CNOs and their composites.

Sample	Onset temperature	Inflection temperature	End temperature
CNOs	500	650	700
Ppy	220	–	600
CNOs/Ppy	230	635	680
CNOs/SDS/Ppy	225	645	685

1000 °C (Supporting Information, Figure S1). Ppy exhibits a gradual mass loss in the temperature range from 30 to 220 °C and from 220 to 600 °C (Figure 2b, curve 2). The complete decomposition of Ppy occurs around 600 °C (Figure 2a, curve 2; see also Table 1). Similar characteristics were observed for both composites: CNOs/Ppy and CNOs/SDS/Ppy, and are assigned to the degradation of the polymer backbone and of the carbon nanostructures. These results also indicate that the CNO/Ppy and CNOs/SDS/Ppy composites are fairly stable up to a temperature of around 220 °C and then start to decompose (see Table 1). Comparison of the thermogravimetric analyses for both composites under different atmospheres clearly shows that degradation in an air atmosphere arises from their combustion (Figure 2; Supporting Information, Figure S1). As shown in Figure 2a, the TGA curves clearly showed that the mass of Ppy decreased in the composites (see curves 3 to 4) and confirmed the presence of the polymer layer on the carbon nanostructure surfaces.

Figure 3 shows the Fourier transform IR (FTIR) spectra of pristine CNOs, PPy, and two CNOs/PPy, and CNOs/SDS/PPy composites. The characteristic peaks around 1530–1540 cm^{-1} and 1460 cm^{-1} are due to the symmetric and unsymmetric stretching modes of the pyrrole rings, respectively.[56] The bands in the range between 1024–1036 cm^{-1} and 1290–1298 cm^{-1} were attributed to C–H deformation vibrations and C–N stretching vibrations, respectively.[57] The peaks near 1160 cm^{-1} in the composites and at 1172 cm^{-1} in the pristine Ppy indicate the doping state of the polymer. The bands in the range between 770–785 cm^{-1} and 850–900 cm^{-1} verify the presence of polymerized pyrrole.[58] These FTIR spectra confirm that Ppy was indeed deposited on the CNO surfaces.

To evaluate the electrochemical performance of the 3D nanostructured CNO composites as supercapacitor electrodes, cyclic voltammetry (CV) studies were performed using a three-electrode configuration. CVs were employed to evaluate the electrochemical performance of the modified electrodes with the CNOs/Ppy and CNOs/SDS/Ppy composites, and pristine CNOs and Ppy for comparison.

It has been shown that the capacitive properties of various porous forms of carbon electrodes depend on the time of the double-layer charging. The effect of the supporting electrolyte on the electrochemical properties of the CNO films was investi-

© 2015 Wiley-VCH Verlag GmbH & Co. KGaA, Weinheim

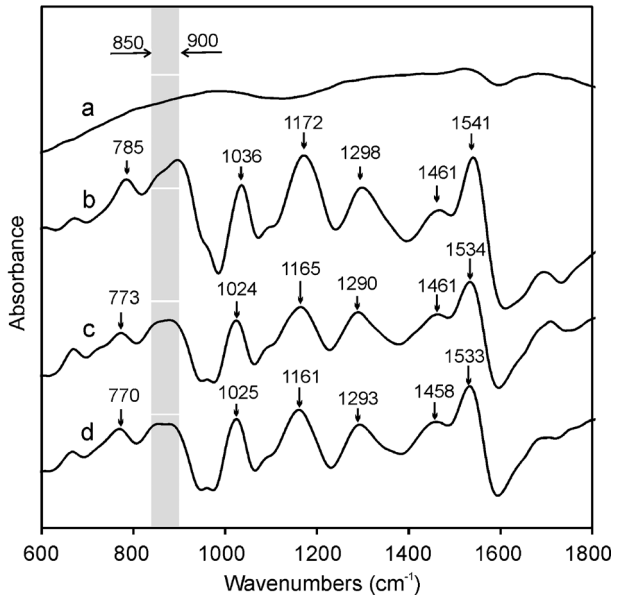

Figure 3. FTIR spectra of a) CNOs, b) PPy, c) CNOs/PPy, and d) CNOs/SDS/PPy. Spectra are offset vertically for clarity.

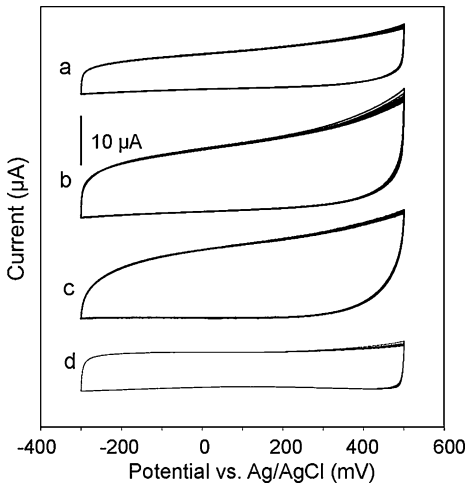

Figure 4. Multicyclic voltammograms of the CNOs films in 0.1 M a) $TBAClO_4$, b) $TBABF_4$, c) $TBAPF_6$, and d) $LiClO_4$. The sweep rate was 20 mV s^{-1}. Voltammograms are offset vertically for clarity.

gated (Figure 4). The films were deposited on the electrode surface by drop coating. A 10 μL aliquot of the dichloromethane solution containing CNOs (1.5 mg mL^{-1}) was dispensed onto the electrode surface. After solvent evaporation in an argon atmosphere, the electrode remained coated with a relatively porous film of the carbon nanostructures. The films were stable and conductive in the potential window ranging from −300 to +500 mV vs. Ag/AgCl (Figure 4). There are two processes responsible for the influence of the supporting electrolyte on the CNOs film capacitance: 1) the degree of counterion penetration in the films, and 2) the structure of the double layer on the CNO surface and electrolyte solution.[59] In the absence of specific adsorption, both effects depend mainly on the size of the supporting electrolyte ions. Multicyclic voltammograms presented in Figure 4 indicate that the charge–discharge processes of the films are accompanied by the transport of the supporting electrolyte from the solution to the film in order to maintain the film electroneutrality.

Figure 5 panel (1) shows the voltammetric responses of the pristine CNOs, the CNOs/Ppy, and CNOs/SDS/Ppy electrodes at

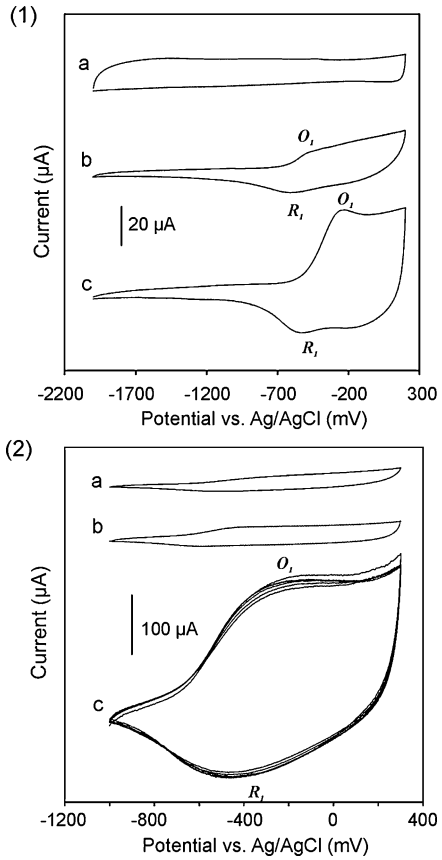

Figure 5. Cyclic voltammograms in MeCN with the addition of 1) 0.1 M $TBAPF_6$ of GCE covered with a) CNOs, b) Ppy, c) CNOs/Ppy; 2) 0.1 M $TBAClO_4$ of GCE covered with a) Ppy, b) CNOs/Ppy, c) CNOs/SDS/Ppy. The sweep rate was 100 mV s^{-1}. Voltammograms are offset vertically for clarity.

scan rates of 100 mV s^{-1}. Voltammograms were recorded for the same mass of material deposited on the electrode surfaces (4.5 μg). After polymer or composite deposition on the GCE electrode (5 μL of active material dispersed in dichloromethane solution) and solvent evaporation, the modified electrodes were transferred to acetonitrile (MeCN) solutions containing 0.1 M tetra(*n*-butyl)ammonium hexafluorophosphate ($TBAPF_6$) or tetra(*n*-butyl)ammonium perchlorate ($TBAClO_4$), and cyclic voltammograms were recorded (panel (1) and (2), respectively). In contrast to the CV curves for pristine CNOs (Figure 5a, panel (1)), that show almost pseudorectangular cathodic and anodic profiles, the CV curves of the CNO composites show electrochemical activity (capacitive faradaic contributions, oxidation and reoxidation process) at potentials less positive than ca. −500 mV (vs. Ag/AgCl) owing to the Ppy backbone electrooxidation. In all cases, films are electrochemically oxidized or reoxidized during potential cycling. For all of the studied com-

© 2015 Wiley-VCH Verlag GmbH & Co. KGaA, Weinheim

posites (CNOs/Ppy and CNOs/SDS/Ppy) in the different tetra(alkyl)ammonium anion solutions (Figure 5), the electrochemical behavior of the deposited films was reversible. The peak potential for the oxidation (O_1) process is shifted anodically by about 300 mV for CNOs/Ppy (Figure 5c, panel (1)) and CNOs/SDS/Ppy (Figure 5c, panel (2)). In this case, an effect due to the supporting electrolyte is observed. The charge for the oxidation of the films increases with a decrease in the size of the anion of the supporting electrolyte. Multicyclic voltammograms presented in Figure 5 indicate that the charge–discharge processes of the films are accompanied by the transport of the supporting electrolyte from the solution to the film to maintain the film electroneutrality. The shape of the voltammograms remains unchanged (Figure 5c, panel (2)). The mechanical and electrochemical stability of the films are important factors to determine the potential practical application of the materials. It was found that mutlicyclic voltammograms recorded for CNOs/polymer composite films are fairly stable in MeCN solution in the potential range between −2000 and +200 mV vs. Ag/AgCl (Figure 5). Tests were conducted using over 500 cycles in a three-electrode system and the resulting capacitive currents as a function of cycling numbers are shown in Figure 6. The CNO/SDS/Ppy electrodes exhibit a long-term

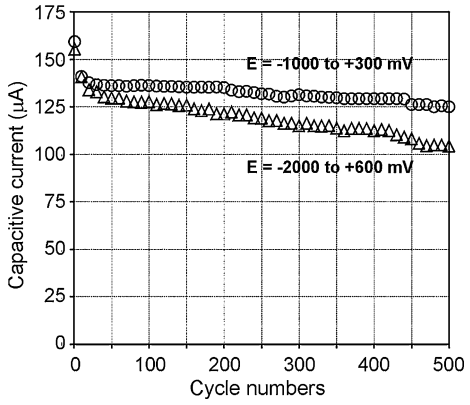

Figure 6. Performances measured at a scan rate of 100 mV s^{-1} for 500 cycles in MeCN and 0.1 M $TBAClO_4$ of GCE covered with CNOs/SDS/Ppy in E from (○) −1000 to +300 mV and (△) −2000 to +600 mV, vs. Ag/AgCl.

cycling stability, retaining ca. 80% and 65% of their initial capacitive current after 500 cycles, for two different potential ranges between −1000 and +300 mV and −2000 and +600 mV vs. Ag/AgCl, respectively. A decrease of the specific capacitance can be attributed to the partial dissolution of the active material and to mechanical failures.

The films formed from the composites with carbon materials, show much higher mechanical and electrochemical stability than films obtained from pristine Ppy. The specific capacitance (C_s) of the electrodes can be estimated from the CV curves using Equation (1), where E_1, E_2 are the cut off potentials in cyclic voltammetry; *i(E)* is the instantaneous current; *i(E)dE* is the total voltammetric charge obtained by integration of the positive and negative sweeps in the cyclic voltammograms, *v* is scan rate, and *m* is the mass of the sample.[5,60]

$$C_S = \frac{\int_{E1}^{E2} i(E)de}{2\nu m(E2 - E1)} \quad (1)$$

The specific capacitance of carbon nanostructures and their composites were calculated from the CVs using [Eq. (1)] for a potential range where the polymer is conducting. These values are collected in Table 2.

Table 2. Specific capacitance of investigated materials in acetonitrile.

Materials	Specific capacitance [F g^{-1}]	
	Integration ΔE[a,b]	*I–v* (slope) E_1 (+100 mV)[b,g]
CNOs	15[e,i]	17[i]
	27[e,k]	30[k]
	33[e,h]	37[h]
	21[e,j]	21[j]
CNOs/Ppy	84[h]	84[h]
	43[i]	44,[i,b] 56,[i,c] 59,[i,d] 65,[i,e] 77[i,f]
CNOs/SDS/Ppy	384[i]	378,[i,b] 490,[i,c] 530,[i,d] 652,[i,e] 805[i,f]
	213[j]	213[j]

[a] The specific capacitance (C_s) was calculated according to [Eq. (1)] in which ΔE is the integration potential range (−100 to +200 mV). Sweep rates: [b] 100; [c] 75; [d] 50; [e] 20 and [f] 5 mV s^{-1}. [g] The specific capacitance (C_s) was calculated according to [Eq. (2)] from the slope of the *I–v* plots. Supporting electrolytes (concentration 0.1 M): [h] $TBAPF_6$; [i] $TBAClO_4$; [j] $LiClO_4$; [k] $TBABF_4$.

The voltammetric behavior of CNOs, CNOs/Ppy, and CNOs/SDS/Ppy films in acetonitrile solution at different sweep rates was investigated. A linear dependence of the total current with the potential sweep rates was expected. The capacitive current, i_c, is given by the following equation:[60]

$$i_c = C_S \nu m \quad (2)$$

where *m* is the mass of material deposited on the electrode surface. The values of the specific capacitances calculated from the dependence of the current with the scan rate for the pristine CNOs, and modified by polypyrrole, are collected in Table 2. A linear dependence of the capacitive current with the sweep rate over a large sweep rate range is observed only for the CNO films. For this electrode, the voltammetric currents are directly proportional to the scan rates, indicating an ideally capacitive behavior.[36,61]

The cathodic sweeps of the cyclic voltammetry curves are not completely symmetric with their corresponding anodic sweeps in the composite electrodes.[62] Supercapacitors involving Faradaic reactions exhibit polarization, and ideal reversible behavior cannot be realized kinetically for the positive and negative cycles.[63] The specific capacitance decreases when the scan rate increases from 5 to 100 mV s^{-1} (Table 2). Electrolyte diffusion within the porous electrode also contributes to the kinetic irreversibility of the redox reaction. A decrease in capacitance is attributed to incomplete redox conversions at higher scan rates, which are due to the diffusion effect of ions

© 2015 Wiley-VCH Verlag GmbH & Co. KGaA, Weinheim

within the electrode. It suggests that parts of the electrode surface are inaccessible at high charge–discharge rates. For the slowest scan rates, these effects not be observed. The highest specific capacitance, equal to about 800 $F g^{-1}$, was obtained for the CNOs/SDS/Ppy composites at 5 $mV s^{-1}$. The results presented above also indicate that the CNOs/SDS/Ppy composites show much higher electrochemical activity than CNOs/Ppy (Table 2), which is due to the higher homogeneity of the CNOs/SDS/Ppy composites.

Electrochemical preparation and characterization of CNOs/PPy composites

Electrochemical deposition techniques provide better control of the deposited redox material mass on the carbon surfaces than chemical synthesis methods. The current trend in supercapacitor development involves the switch from an aqueous electrolyte, which has a low operating voltage of 1 V (owing to the decomposition of water) to a non-aqueous medium which allow a much higher voltage window of about 2.5 V. The most recent supercapacitors available in the market use electrolytes based on aprotic solvents, typically acetonitrile or carbonate-based solvents. In our studies both types of solvents, protic and aprotic, were used for the electrochemical deposition of Py.

It can be clearly be seen from the images in Figure 7 that the Ppy particles have spherical structures. Increasing the time of polymerization caused the formation of a hierarchical multilayer of porous nanospheres (Figures 7e and 7g). During the deposition of polymer on the carbon matrix, the Ppy layers formed compact and smooth structures at the center of the electrode (structure 1 in Figures 7e and 7f) with more developed 3D spherical structures of Ppy on the edges of the electrode surface (structure 2 in Figures 7e and 7g). The morphologies depend also on the solutions (Supporting Information, Figure S2) and the supporting electrolytes used (Supporting Information, Figures S3–S6). In a solution containing $LiClO_4$, three-dimensional crystals of the supporting electrolytes formed as needles (Figure 7a; Supporting Information, Figures S3 and S4). The number of these crystals and their size increases with an increase of the times of the electrodepositions (Supporting Information, Figures S3 and S4).

The specific capacitance of the film can be calculated from the relationship between the pseudocapacitance current and the mass of the electroactive materials deposited on the electrode surface. The piezoelectric microgravimetric (EQCM) studies for the electrodeposition of Ppy (Supporting Information, Figure S7) and its composites containing carbon nano-onions were performed in an aqueous (Figures 8 and 9a) or organic (Figure 9b) solution. The decrease of the frequency of the quartz crystal at potentials in the range −1200 and 1200 mV (vs. Ag/AgCl) is related to the deposition of a new solid phase on the Au/quartz electrode surface (Figure 8). These potentials correspond to increases of the oxidation current of pyrrole under voltammetric conditions. Therefore, oxidation of py results in the electrodeposition of a new solid phase (polypyrrole) on the electrode surface.

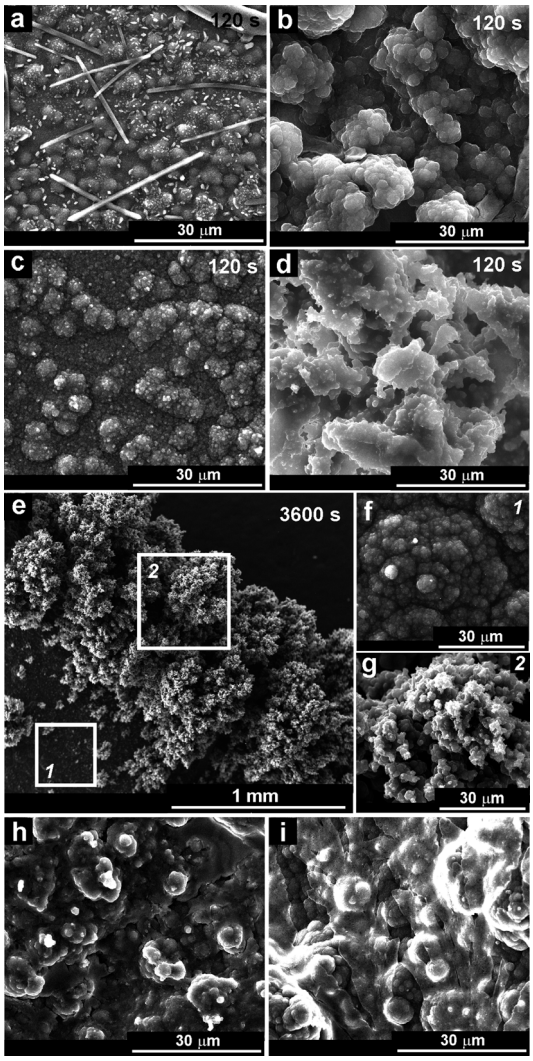

Figure 7. SEM images of a) PPy and b), e), f), g) CNOs/PPy in $LiClO_4$; c) Ppy and d) CNOs/PPy in $TBAClO_4$ (MeCN, 1% H_2O, 0,1 M Ppy $E = 0.85$ V vs. Ag/AgCl); potentiostatic polymerization at a), b), c), d) $t = 120$ s and e), f), g) $t = 3600$ s. h), i) SEM images of CNOs/Ppy obtained by CVs in 0.1 M Na_2SO_4, in E from −1200 to 1200 mV (vs. Ag/AgCl) h) 10 and i) 60 cycles.

The total change in mass increases with every cycle indicating that the amount of film material deposited on the electrode increases (Figures 8 and 9a; Supporting Information, Figure S7). The mass of the polymer deposited on the electrode surface of the composites was calculated from EQCM measurements (Table 3). From the frequency changes, Δf, the mass of the polymeric material was calculated using the Sauerbrey equation:[64]

$$\Delta m = 17.7\,\Delta f \qquad (3)$$

The mass changes, Δm ($ng\,Hz^{-1}\,cm^{-2}$), indicate differences in the yield of polymer formation at the different experimental conditions, as well as on the nature of the electrode surface, pristine Au quartz electrodes (Supporting Information, Figure S7), or Au quartz electrodes with CNO films (Figure 8).

© 2015 Wiley-VCH Verlag GmbH & Co. KGaA, Weinheim

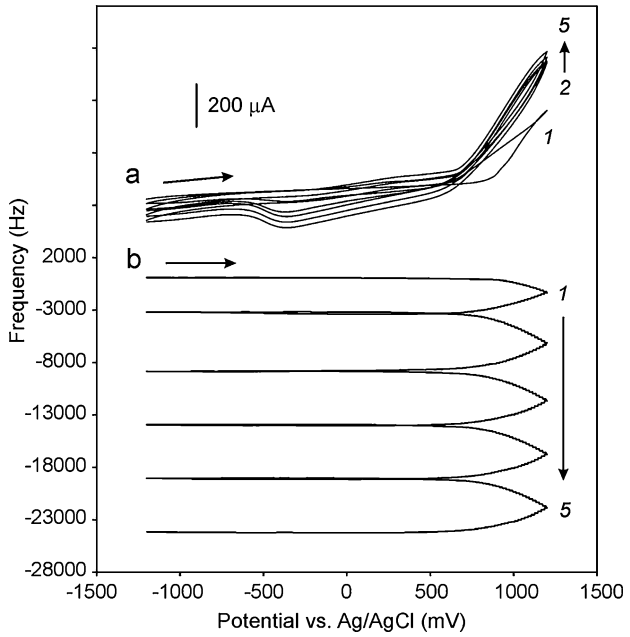

Figure 8. a) Multicyclic voltammograms and b) curves of frequency changes vs. potential simultaneously recorded at the Au/quartz electrode/CNOs in 0.1 M Na_2SO_4 containing 0.1 M pyrrole. The scan rate was 50 mV s^{-1}.

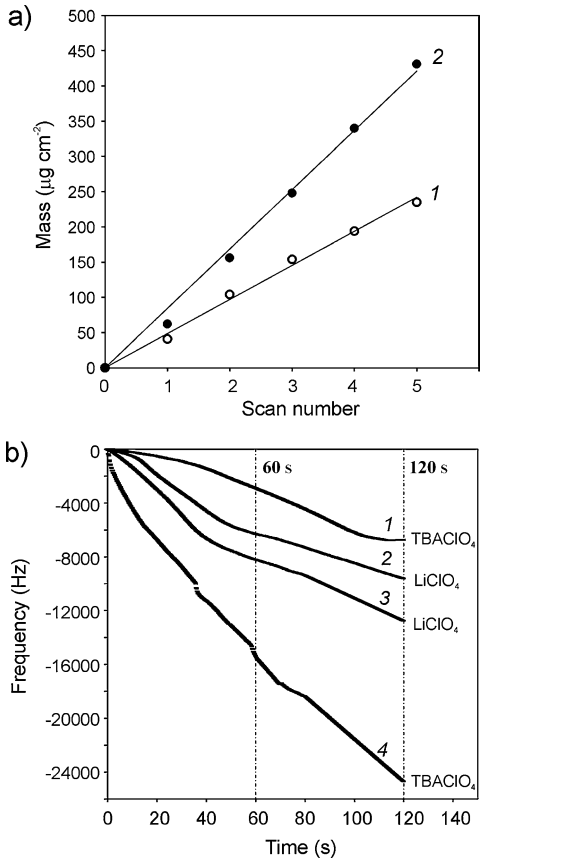

Figure 9. a) Mass values of Ppy deposited on the 1) Au/quartz or 2) Au/quartz/CNOs electrode in 0.1 M Na_2SO_4. The range of potential from −1200 mV to 1200 mV (vs. Ag/AgCl); v = 50 mV s^{-1}. b) Curves of potentiostatic deposition of polypyrrole recorded at the 1), 2) Au/quartz electrode or 3), 4) Au/quartz/CNOs electrode in an MeCN (1% H_2O) solution containing 0.1 M $LiClO_4$ or 0.1 M $TBAClO_4$, E = 0.85 V (vs Ag/AgCl). The pyrrole concentration was 0.1 M.

The relationship between the mass values and the scan numbers/time of deposition of polymer on the electrode surface is presented in Figure 9. At low cycle numbers (Figure 9a) and time (Figure 9b) the mass (μg cm^{-2}) of polypyrrole deposited on the electrode surface increased linearly with time. These results were also used to calculate the specific capacitance of the deposited polymers (see Table 3). Because of diffusion control, the high-capacitance performance of CNOs/PPy was obtained in $TBAClO_4$. An increase of the amount of polypyrrole deposited on the electrode surface, pristine or modified with CNOs (see Table 3) results in an increase of the film resistance for the thicker films.

The capacitance performance of the CNOs/PPy electrodes was investigated by cyclic voltammetry (Figure 10). Electrochemically grown polymers on CNO films exhibit typical capacitive behavior in the potential range between −200 to +600 mV vs. Ag/AgCl. The CVs exhibit almost rectangular and symmetric shapes, suggesting fast reversible Faradaic reactions and ideal capacitive behavior. To examine the effect of the supporting electrolyte on the CNOs/Ppy electrodes, voltammograms were recorded in acetonitrile solution containing $TBAClO_4$ or $LiClO_4$. The processes are accompanied by cation transport from the solution to the composites. This ion doping process limits the amount of polymer that is oxidized. Charges for the capacitive current of the films increase with a decrease in the size of the cation supporting electrolyte (Table 3). The shape of the voltammograms remains unchanged.

From the comparisons, we conclude that the chemical and electrochemical methods, are flexible and enable control of:

Table 3. Specific capacitance of investigated materials in MeCN base on EQCM studies.

Materials	E [mV][a] vs. Ag/AgCl		t = 60 s[c]				t = 120 s[c]			
	Na_2SO_4		$LiClO_4$		$TBAClO_4$		$LiClO_4$		$TBAClO_4$	
	Δm [μg cm^{-2}]	C_S[b,d] [F g^{-1}]	Δm [μg cm^{-2}]	C_S[b,d] [F g^{-1}]	Δm [μg cm^{-2}]	C_S[b,d] [F g^{-1}]	Δm [μg cm^{-2}]	C_S[b,d] [F g^{-1}]	Δm [μg cm^{-2}]	C_S[b,d] [F g^{-1}]
Au/Ppy	7.4	796	3.5	413	1.6	180	5.4	329	3.8	378
CNOs/Ppy	13.5	331	4.6	1064	8.6	194	7.1	1320	13.7	428

[a] From −1200 to +1200 mV. [b] The specific capacitance (C_s) was calculated according to [Eq. (1)] in which ΔE is the integration potential range. Integration ΔE from −100 to +200 mV vs. Ag/AgCl. [c] Potentiostatic deposition of Ppy at E = 850 mV vs. Ag/AgCl. [d] Sweep rates was 20 mV s^{-1}.

© 2015 Wiley-VCH Verlag GmbH & Co. KGaA, Weinheim

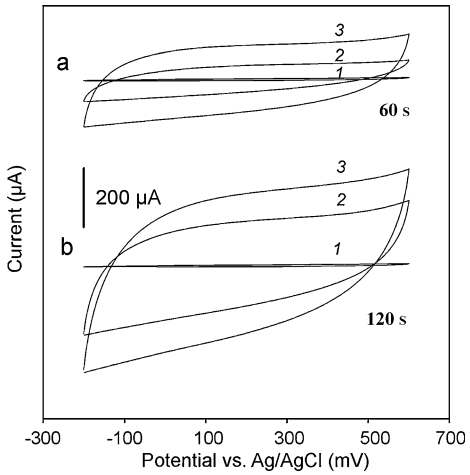

Figure 10. Multicyclic voltammograms of the 1) CNOs, and 2), 3) CNOs/Ppy films in 0.1 M 1), 2) $TBAClO_4$, and 3) $LiClO_4$. The scan rate was 20 mV s^{-1}. Ppy was deposited by potentiostatic polymerization at $E = 850$ mV vs. Ag/AgCl, during a) 60 s and b) 120 s.

1) the homogeneity of the composites; 2) the film thickness by adjusting deposition time of the polymers on the carbon surface; and 3) the electrochemical properties by using different supporting electrolytes and solutions.

Conclusion

Composites containing carbon nano-onions were prepared by chemical or electrochemical polymerization of pyrrole on the carbon material surface. The introduction of Ppy on the carbon nano-onions surface significantly enhanced the electrochemical properties of the carbon materials due to the introduction of pseudocapacitive characteristics to the composites. The materials exhibit porous structures. All materials are electrochemically active and exhibit good electrochemical stabilities, especially these including carbon nanomaterials. The CNOs/Ppy and CNOs/SDS/Ppy composites also have fast current responses upon potential switching. The materials exhibit good capacitive properties, as high as 1320 F g^{-1} for the CNOs/Ppy bilayer in 0.1 M $LiClO_4$, and ca. 800 F g^{-1} in 0.1 M $TBAClO_4$ for the homogenous CNOs/SDS/Ppy composite. Our study thus presents a simple and effective way to fabricate CNOs/Ppy and CNOs/SDS/Ppy composites with good electrochemical properties as promising materials for supercapacitors.

Experimental Section

Materials

The pyrrole used for chemical or electrochemical polymerization was stored at 4 °C prior to use. The following chemicals were used as received: NaCl (100%, POCH), $LiClO_4$ (99%, Fluka), Na_2SO_4 (97%, POCH), $FeCl_3$ (98%, Merck Schuchardt), $NaClO_4$ (98%, Sigma–Aldrich), $TBAClO_4$ (99%, Fluka), $TBAPF_6$ (99%, Fluka), $TBABF_4$ (99%, Fluka), CH_2Cl_2 (> 99,5%, POCH), H_2SO_4 (95%, POCH), MeCN (99,8%, Sigma–Aldrich) were analytically pure and used as purchased without any further treatment. All aqueous solutions were prepared with deionized water.

Commercially available nanodiamond powder (Carbodeon μDiamond Molto) with a crystal size 4–6 nm, and nanodiamond content ≥ 97 wt%, was used for preparation of CNOs. Annealing of ultradispersed nanodiamonds was performed at 1650 °C under a He atmosphere with a heating ramp of 20 °C min^{-1}.[31] The final temperature was maintained for one hour, then the material was slowly cooled to room temperature over a period of one hour. The furnace was opened, and the transformed CNOs were annealed in air at 400 °C to remove any amorphous carbon.

Methods

The studied films were imaged by secondary electron SEM with the use of an S-3000N scanning electron microscope from FEI (Tokyo, Japan). The accelerating voltage of the electron beam was either 15 or 20 keV and the working distance was 10 mm. Transmission electron microscope images were recorded using the FEI Tecnai instrument. The accelerating voltage of the electron beam was 200 keV. Thermogravimetric experiments were performed using an SDT 2960 simultaneous TGA-DTG-DTA (TA Instruments company). The spectra were collected at 10 °C min^{-1} in an air atmosphere (100 mL min^{-1}).

The Fourier transform IR (FTIR) spectra were recorded in the range between 4000 and 100 cm^{-1} with a Nicolet 6700 Thermo Scientific spectrometer at room temperature under N_2 atmosphere. The spectra were collected with a resolution of 4 cm^{-1}. All of the spectra were corrected with conventional software to cancel the variation of the analyzed thickness with the wavelength.

Voltammetric experiments were performed using a potentiostat/galvanostat model AUTOLAB (Utrecht, The Netherlands) with a three-electrode cell. Impedance spectroscopy (EIS) measurements were performed on an AUTOLAB (Utrecht, The Netherlands) computerized electrochemistry system equipped with a PGSTAT 12 potentiostat and FRA response analyzer expansion card with a three-electrode cell. The AUTOLAB system was controlled with the GPES 4.9 software of the same manufacturer. A glassy carbon disk (GCE) with a diameter of 1.6 mm (Bioanalytical Systems Inc.) was used as the working electrode. The surface of the electrode was polished using extra fine carborundum paper (Buehler) followed by 0.3 μm alumina and 0.25 μm diamond polishing compound (Metadi II, Buehler). The electrode was then sonicated in water in order to remove traces of alumina from the metal surface, washed with water, and dried. The counter electrode was made from platinum mesh (0.25 mm) and was cleaned by heating in a flame for approximately 30 seconds. A silver wire with deposited AgCl (3 M KCl) served as the reference electrode.

Simultaneous voltammetric and piezoelectric microgravimetry experiments were carried out with a home-made built potentiostat and an electrochemical quartz crystal microbalance, EQCM 5510 (Institute of Physical Chemistry, Warsaw, Poland). Plano-convex quartz crystals were used. The 14 mm diameter AT-cut, plano-convex quartz crystals with a 5 MHz resonant frequency were obtained from Omig (Warsaw, Poland). A 100 nm gold film, which was vacuum-deposited on the quartz crystal, served as the unpolished working electrode. The sensitivity of the mass measurement calculated from the Saurbrey equation was 17.7 ng Hz^{-1} cm^{-2}.

© 2015 Wiley-VCH Verlag GmbH & Co. KGaA, Weinheim

Acknowledgements

We appreciate the assistance of Monika Wysocka-Zolopa with the EQCM measurements. We gratefully acknowledge the financial support of the National Science Foundation, Poland, grant #2012/05/E/ST5/03800 to M.E.P.-B. L.E. thanks the Robert A. Welch Foundation for an endowed chair, grant #AH-0033 and the US NSF, grant: DMR-1205302. SEM, TEM, FTIR, and the potentiostat/galvanostat were funded by the European Funds for Regional Development and the National Funds of Ministry of Science and Higher Education, as part of the Operational Programme Development of Eastern Poland 2007–2013, project: POPW.01.03.00-20-034/09-00.

Keywords: carbon nano-onions · composite materials · nanomaterials · polypyrrole · supercapacitors

[1] a) R. B. Rakhi, W. Chen, H. N. Alshareef, *J. Mater. Chem.* **2012**, *22*, 5177 – 5183; b) C. Xu, B. Xu, Y. Gu, Z. Xiong, J. Sun, X. S. Zhao, *Energy Environ. Sci.* **2013**, *6*, 1388 – 1414.

[2] J. Breczko, M. E. Plonska-Brzezinska, L. Echegoyen, *Electrochim. Acta* **2012**, *72*, 61 – 67.

[3] M. E. Plonska-Brzezinska, D. M. Brus, A. Molina-Ontoria, L. Echegoyen, *RSC Advances* **2013**, *3*, 25891 – 25901.

[4] J. Breczko, K. Winkler, M. E. Plonska-Brzezinska, A. Villalta-Cerdas, L. Echegoyen, *J. Mater. Chem.* **2010**, *20*, 7761 – 7768.

[5] a) B. B. Owens, T. Osaka, *J. Power Sources* **1997**, *68*, 173 – 186; b) G. Wang, L. Zhang, J. Zhang, *Chem. Soc. Rev.* **2012**, *41*, 797 – 828; c) E. Frackowiak, F. Beguin, *Carbon* **2001**, *39*, 937 – 950; d) E. Frackowiak, *Phys. Chem. Chem. Phys.* **2007**, *9*, 1774 – 1785.

[6] S. Bose, T. Kuila, A. K. Mishra, R. Rajasekar, N. H. Kim, J. H. Lee, *J. Mater. Chem.* **2012**, *22*, 767 – 784.

[7] a) A. G. Pandolfo, A. F. Hollenkamp, *J. Power Sources* **2006**, *157*, 11 – 27; b) J. Chmiola, G. Yushin, Y. Gogotsi, C. Portet, P. Simon, P. L. Taberna, *Science* **2006**, *313*, 1760 – 1763; c) M. D. Levi, G. Salitra, N. Levy, D. Aurbach, *Nat. Mater.* **2009**, *8*, 872 – 875.

[8] a) Z. A. Hu, Y. L. Xie, Y. X. Wang, H. Y. Wu, Y. Y. Yang, Z. Y. Zhang, *Electrochim. Acta* **2009**, *54*, 2737 – 2741; b) M.-W. Xu, D.-D. Zhao, S.-J. Bao, H.-L. Li, *J. Solid State Electrochem.* **2007**, *11*, 1101 – 1107; c) B. Wang, J. Park, C. Wang, H. Ahn, G. Wang, *Electrochim. Acta* **2010**, *55*, 6812 – 6817; d) J. Yan, T. Wei, W. Qiao, B. Shao, Q. Zhao, L. Zhang, Z. Fan, *Electrochim. Acta* **2010**, *55*, 6973 – 6978; e) M.-S. Wu, C.-Y. Huang, K.-H. Lin, *J. Power Sources* **2009**, *186*, 557 – 564.

[9] J. P. Ferraris, M. M. Eissa, I. D. Brotherson, D. C. Loveday, A. A. Moxey, *J. Electroanal. Chem.* **1998**, *459*, 57 – 69.

[10] a) T. Kuillaa, S. Bhadrab, D. Yaoa, N. H. Kimc, S. Bosed, J. H. Lee, *Prog. Polym. Sci.* **2010**, *35*, 1350 – 1375; b) H. Pan, J. Li, Y. P. Feng, *Nanoscale Res. Lett.* **2010**, *5*, 654 – 668; c) Z. Spitalsky, D. Tasis, K. Papagelis, C. Galiotis, *Prog. Polym. Sci.* **2010**, *35*, 357 – 401; d) Y. Sun, Q. Wu, G. Shi, *Energy Environ. Sci.* **2011**, *4*, 1113 – 1132.

[11] a) F. Fusalba, P. Gouerec, D. Villers, D. Belanger, *J. Electrochem. Soc.* **2001**, *148*, A1 – A6; b) V. Baranauskas, H. J. Ceragioli, A. C. Peterlevitz, J. C. R. Quispe, *J. Phys. Conference Series* **2007**, *61*, 71 – 74; c) H.-P. Cong, X.-C. Ren, P. Wang, S.-H. Yu, *Energy Environ. Sci.* **2013**, *6*, 1185 – 1191; d) L. Wang, X. Lu, S. Lei, Y. Song, *J. Mater. Chem. A* **2014**, *2*, 4491 – 4509; e) T.-M. Wu, Y.-W. Lin, *Polymer* **2006**, *47*, 3576 – 3582.

[12] a) T. Qian, Ch. Yu, S. Wu, J. Shen, *J. Mater. Chem. A* **2013**, *1*, 6539 – 6542; b) J.-G. Wang, Y. Yang, Z.-H. Huang, F. Kang, *J. Mater. Chem.* **2012**, *22*, 16943 – 16949.

[13] C.-C. Hu, X.-X. Lin, *J. Electrochem. Soc.* **2002**, *149*, A1049 – A1057.

[14] a) A. G. MacDiarmid, *Angew. Chem. Int. Ed.* **2001**, *40*, 2581 – 2590; b) C. M. Li, C. Q. Sun, W. Chen, L. Pan, *Surf. Coat. Technol.* **2005**, *198*, 474 – 477; c) X. Q. Cui, C. M. Li, J. F. Zang, Q. Zhou, Y. Gan, H. F. Bao, J. Guo, V. S. Lee, S. M. Moochhala, *J. Phys. Chem. C* **2007**, *111*, 2025 – 2031; d) Q. Zhou, C. M. Li, J. Li, X. Q. Cui, D. Gervasio, *J. Phys. Chem. C* **2007**, *111*, 11216 – 11222; e) Y. Qiao, C. M. Li, S. J. Bao, Q. L. Bao, *J. Power Sources* **2007**, *170*, 79 – 84.

[15] J. C. Thiéblemont, A. Brun, J. Marty, M. F. Planche, P. Calo, *Polymer* **1995**, *36*, 1605 – 1610.

[16] S. Suematsu, Y. Oura, H. Tsujimoto, H. Kanno, K. Naoi, *Electrochim. Acta* **2000**, *45*, 3813 – 3821.

[17] a) C.-C. Hu, C.-H. Chu, *Mater. Chem. Phys.* **2000**, *65*, 329 – 338; b) C.-C. Hu, C.-H. Chu, *J. Electroanal. Chem.* **2001**, *503*, 105 – 116.

[18] H. Fu, Z.-j. Du, W. Zou, H.-q. Li, Ch. Zhang, *J. Mater. Chem. A.* **2013**, *1*, 14943 – 14950; see Ref. [12a].

[19] P. Si, S. Ding, X.-W. Lou, D.-H. Kim, *RSC Advances* **2011**, *1*, 1271 – 1278.

[20] S.-H. Song, D.-S. Han, H.-J. Lee, H.-S. Cho, S.-M. Chang, J.-M. Kim, H. Muramatsu, *Synth. Met.* **2001**, *117*, 137 – 139.

[21] a) E. Frackowiak, V. Khomenko, K. Jurewicz, K. Lota, F. Beguin, *J. Power Sources* **2006**, *153*, 413 – 418; b) P. J. Kinlen, J. Liu, Y. Ding, C. R. Graham, E. E. Remsen, *Macromolecules* **1998**, *31*, 1735 – 1744.

[22] Ch. Yang, P. Liu, T. Wang, *ACS Appl. Mater. Interfaces* **2011**, *3*, 1109 – 1114.

[23] Y. Fang, J. Liu, D. J. Yu, J. P. Wicksted, K. Kalkan, C. O. Topal, B. N. Flanders, J. Wu, J. Li, *J. Power Sources* **2010**, *195*, 674 – 679.

[24] J. Liu, J. An, Y. Ma, M. Li, R. Ma, *J. Electrochem. Soc.* **2012**, *159*, A828 – A833.

[25] P. A. Mini, A. Balakrishnan, S. V. Nair, K. R. V. Subramanian, *Chem. Commun.* **2011**, *47*, 5753 – 5755.

[26] S. Iijima, *J. Cryst. Growth.* **1980**, *50*, 675 – 683.

[27] R. Al-Jishi, G. Dresselhaus, *Phys Rev B* **1982**, *26*, 4514 – 4522.

[28] J. Suehiro, K. Imasaka, Y. Ohshiro, G. Zhou, M. Hara, N. Sano, *Jpn. J. Appl. Phys.* **2003**, *42*, L1483 – L1485.

[29] V. V. Roddatis, V. L. Kuznetsov, Y. V. Butenko, D. S. Sua, R. Schlögl, *Phys. Chem. Chem. Phys.* **2002**, *4*, 1964 – 1967.

[30] D. M. Ugarte, *Nature* **1992**, *359*, 707 – 709.

[31] a) E. Thune, Th. Cabioc'h, M. Jaouen, F. Bodart, *Phys. Rev. B* **2003**, *68*, 115434; b) Th. Cabioc'h, E. Thune, M. Jaouen, *Phys. Rev. B* **2002**, *65*, 132103; c) R. Lamber, N. I. Jeager, G. Schultz-Ekloff, *Surf. Sci.* **1988**, *197*, 402 – 414.

[32] V. L. Kuznetsov, A. L. Chuvilin, Y. V. Butenko, I. Y. Malkov, V. M. Titov, *Chem. Phys. Lett.* **1994**, *222*, 343 – 348.

[33] N. Sano, H. Wang, I. Alexandrou, M. Chhowalla, K. B. K. Teo, G. A. Amaratunga, K. Iimura, *J. Appl. Phys.* **2002**, *92*, 2783 – 2788.

[34] a) Ch. Zhang, J. Li, E. Liu, Ch. He, Ch. Shi, X. Du, R. H. Hauge, N. Zhao, *Carbon* **2012**, *50*, 3513 – 3521; b) C. N. He, N. Q. Zhao, C. S. Shi, S. Z. Song, *J. Alloys Compounds* **2009**, *484*, 6 – 11; c) C. N. He, C. S. Shi, X. W. Du, J. J. Li, N. Q. Zhao, *J. Alloys Compounds* **2008**, *452*, 258 – 262; d) X. H. Chen, F. M. Deng, J. X. Wang, H. S. Yang, G. T. Wu, X. B. Zhang, J. C. Peng, W. Z. Li, *Chem. Phys. Lett.* **2001**, *336*, 201 – 204.

[35] a) A. S. Rettenbacher, B. Elliott, J. S. Hudson, A. Amirkhanian, L. Echegoyen, *Chem. Eur. J.* **2006**, *12*, 376 – 387; b) A. Palkar, F. Melin, C. M. Cardona, B. Elliott, A. K. Naskar, D. D. Edie, *Chem. Asian J.* **2007**, *2*, 625 – 633.

[36] J. K. McDonough, A. I. Frolov, V. Presser, J. Niu, Ch. H. Miller, T. Ubieto, M. V. Federov, Y. Gogotsi, *Carbon* **2012**, *50*, 3298 – 3309.

[37] D. Pech, M. Burnett, H. Durou, P. Huang, V. Mochalin, Y. Gogotsi, P.-L. Taberna, P. Simon, *Nat. Nanotechnol.* **2010**, *5*, 651 – 654.

[38] C. Portet, J. Chmiola, Y. Gogotsi, S. Park, K. Lian, *Electrochim Acta* **2008**, *53*, 7675 – 7680.

[39] Y. Gao, Y. S. Zhou, M. Qian, X. N. He, J. Redepenning, P. Goodman, H. M. Li, L. Jiang, Y. F. Lu, *Carbon* **2013**, *51*, 52 – 58.

[40] N. Keller, N. I. Maksimova, V. V. Roddatis, M. Schur, G. Mestl, Y. V. Butenko, V. L. Kuznetsov, R. Schlögl, *Angew. Chem. Int. Ed.* **2002**, *41*, 1885 – 1888; *Angew. Chem.* **2002**, *114*, 1962 – 1966.

[41] S. Sek, J. Breczko, M. E. Plonska-Brzezinska, A. Z. Wilczewska, L. Echegoyen, *ChemPhysChem* **2013**, *14*, 96 – 100.

[42] M.-S. Wang, D. Goldberg, Y. Bando, *ACS Nano* **2010**, *4*, 4396 – 4402.

[43] W. Gu, N. Peters, G. Yushin, *Carbon* **2013**, *53*, 292 – 301.

[44] F.-D. Han, B. Yao, Y.-J. Bai, *J. Phys. Chem. C* **2011**, *115*, 8923 – 8927.

[45] E. Koudoumas, O. Kokkinaki, M. Konstantaki, S. Couris, S. Korovins, P. Detkov, V. Kuznetsov, S. Pimenov, V. Pustovoi, *Chem. Phys. Lett.* **2002**, *357*, 336 – 340.

[46] S. Tomita, M. Fujii, S. Hayashi, *Phys. Rev. B* **2002**, *66*, 245424.

[47] V. L. Kuznetsov, S. I. Moseenkov, K. V. Elumeeva, T. V. Larina, V. F. Anufrienko, A. I. Romanenko, O. B. Anikeeva, E. N. Tkachev, *Phys. Status Solidi B* **2011**, *248*, 2572 – 2576.

© 2015 Wiley-VCH Verlag GmbH & Co. KGaA, Weinheim

[48] a) L. Joly-Pottuz, N. Matsumoto, H. Kinoshita, B. Vacher, M. Belin, G. Montagnac, J. M. Martin, N. Ohmae, *Tribology Int.* **2008**, *41*, 69 – 78; b) L. Joly-Pottuz, B. Vacher, N. Ohmae, J. M. Martin, T. Epicier, *Tribol. Lett.* **2008**, *30*, 69 – 80.
[49] A. Hirata, M. Igarashi, T. Kaito, *Tribology Inter.* **2004**, *37*, 899 – 905.
[50] V. L. Kuznetsov, I. L. Zilberberg, Y. V. Butneko, A. L. Chuvilin, B. Segall, *J Appl Phys* **1999**, *86*, 863 – 870.
[51] M. E. Plonska-Brzezinska, D. M. Brus, J. Breczko, L. Echegoyen, *Chem. Eur. J.* **2013**, *19*, 5019 – 5024.
[52] J. Luszczyn, M. E. Plonska-Brzezinska, A. Palkar, A. T. Dubis, A. Simionescu, D. T. Simionescu, B. Kalska-Szostko, K. Winkler, L. Echegoyen, *Chem. Eur. J.* **2010**, *16*, 4870 – 4880.
[53] a) A. Łapiński, A. T. Dubis, M. E. Plonska-Brzezinska, J. Mazurczyk, J. Breczko, L. Echegoyen, *Phys. Status Solidi C* **2012**, *9*, 1210 – 1212; b) M. E. Plonska-Brzezinska, J. Breczko, B. Palys, L. Echegoyen, *Chem. Phys. Chem.* **2013**, *14*, 116 – 124; c) M. E. Plonska-Brzezinska, M. Lewandowski, M. Błaszczyk, A. Molina-Ontoria, T. Luciński, L. Echegoyen, *Chem. Phys. Chem.* **2012**, *13*, 4134 – 4141.
[54] a) R. Borgohain, J. Li, J. P. Selegue, Y.-T. Cheng, *J. Phys. Chem. C* **2012**, *116*, 15068 – 15075; b) Y. Wang, S. F. Yu, C. Y. Sun, T. J. Zhu, H. Y. Yang, *J. Mater. Chem.* **2012**, *22*, 17584 – 17588; c) M. V. K. Azhagan, M. V. Vaishampayan, M. V. Shalke, *J. Mater. Chem. A* **2014**, *2*, 2152 – 2159.
[55] a) B. Xu, X. Yang, X. Wang, J. Guo, X. Liu, *J. Power Sources* **2006**, *162*, 160 – 164; b) D. Santiago, G. G. Rodríguez-Calero, A. Palkar, *Langmuir* **2012**, *28*, 17202 – 17210; c) Y. A. Goh, X. Chen, F. M. Yasin, *Chem. Commun.* **2013**, *49*, 5171 – 5173; d) E. Grądzka, K. Winkler, M. Borowska, M. E. Plonska-Brzezinska, L. Echegoyen, *Electrochim. Acta* **2013**, *96*, 274 – 284.
[56] Y. Shi, L. Pan, B. Liu, Y. Wang, Y. Cui, Z. Bao, G. Yu, *J. Mater. Chem. A* **2014**, *2*, 6086 – 6091.
[57] S. Konwer, S. K. Dolui, *Mater. Chem. Phys.* **2010**, *124*, 738 – 743.
[58] Y. C. Liu, Y. T. Lin, *J. Phys. Chem. B* **2003**, *107*, 11370 – 11375.
[59] a) M. Yaniv, A. Soffer, *J. Electrochem. Soc.* **1976**, *123*, 506 – 511; b) J. Koresh, A. Soffer, *J. Electrochem. Soc.* **1977**, *124*, 1379 – 1385.
[60] R. Kötz, M. Carlen, *Electrochim. Acta* **2000**, *45*, 2483 – 2498.
[61] a) D. P. Dubal, D. S. Dhawale, R. R. Salunkhe, C. D. Lokhande, *J. Electroanal. Chem.* **2010**, *647*, 60 – 67.
[62] a) J. S. Newman, C. W. Tobias, *J. Electrochem. Soc.* **1962**, *109*, 1183 – 1191; b) J. M. Lehn, J. P. Sauvage, *Chem. Commun.* **1971**, 440; c) R. de Levie, *Electrochim. Acta* **1964**, *9*, 1231 – 1245.
[63] K. A. Noh, D. W. Kim, C. S. Jin, K. H. Shin, J. H. Kim, J. M. Ko, *J. Power Sources* **2003**, *124*, 593 – 595.
[64] G. Sauerbrey, *Z. Phys.* **1959**, *155*, 206 – 222.

Received: November 18, 2014
Published online on March 3, 2015

© 2015 Wiley-VCH Verlag GmbH & Co. KGaA, Weinheim